Resolution in evaluation of structural elements by using ground-penetrating radar.

V. Perez-Gracia

Departamento de Resistencia de Materiales y Estructuras en la Ingeniería. EUETIB/CEIB. Universidad Politécnica de Cataluña. C/Urgell 187, 08036 Barcelona. E-mail: vega.perez@upc.edu

Abstract. Ground-penetrating radar (GPR) is a non-invasive geophysical technique widely used in civil engineering, archaeology and shallow geology. Radar images of the inner media provides information about inner

1 Introduction

Geophysical prospecting methods use to be non-destructive techniques, based on superficial measurements of the media physical properties. The evaluation of these measured properties provides indirect information about features of the studied media. Ground-penetrating radar is a geophysical and close-range remote sensing technique based on the use of radar pulses to obtain cross-section images of underground features. GPR principles of operation are based on the ability of radio waves and microwaves to penetrate into the material media, from the first few centimetres to many metres, depending on signal frequency and electromagnetic properties of the studied medium. This method based on the emission of very short time domain electromagnetic pulses (1-20 ns) in the lower frequency radar bands (usually 25 MHz - 2.5 GHz). Those waves are detected after suffering a reflection in the electromagnetic discontinuities of the propagation medium. The characteristics of the received signal depend on the electromagnetic properties of the materials, which depend on the type of matter of the medium and their physical properties (mainly water content and porosity). GPR is widely used in non-destructive high-resolution studies, mainly in civil engineering (e.g., Hugenschmidt, 2002; Barnes et al., 2008; Lahouar and Al-Qadi, 2008), archaeology (e.g., Negri and Leucci, 2006; Perez-Gracia et al., 2009); and shallow geology (e.g., Neal and Roberts, 2001).

The evaluation of ancient structures and cultural heritage by means of GPR uses to bring to complex radar imaging due to complexity inherent to these historical constructions. On the other hand, in this kind of studies, it is necessary to obtain an imaging of the subsurface with maximum resolution. Accurate interpretation of radar data and the correct analysis of the information require a wide knowledge of the radar behaviour.

In this paper, the spatial resolution of a 1.6 GHz antenna is determined by means experimental measurements. These lab evaluations allow obtaining values of the horizontal and vertical resolution, as well as the radiated beam of the antenna. Resolution is generally defined as an imaging system's ability to record and display fine detail in a distinguishable manner. Horizontal resolution uses to be considered as the ability to detect lateral changes along a reflector or the capacity to detect two close elements at the same depth as two separate anomalies. This ability also depends on shape of the emitted cone of energy. Vertical resolution could be defined as the capability to detect as separated anomalies, two close targets at different depths, but in the same vertical. This ability depends on the duration of the electromagnetic impulses and the bandwidth of the antenna. Different case studied are also reviewed and considered in order to compare applied to laboratory results.

2 Background theory

Spatial resolution depends on the characteristics of the radar signal and the survey, the EM properties of the studied medium, and the distance from the antenna to the target. The frequencies used, the number of traces or scans over the target, and the spatial antenna beam pattern are the features related to the radar signal and to the survey. Experimental measures, numerical simulations and data processing indicate that, in order to detect a target, a minimum of three scans must be made over the anomalous body Ghasemi and Abrishamian, 2007). Resolution is the highest when the antenna is placed over the surface of the medium, and it decreases as the distance from the antenna to the surface increases (van der Kruk, 2004). We also know that spatial resolution improves as attenuation increases (Daniels, 2004) and that attenuation depends mainly on the frequencies and on the EM properties of the medium. In spite of these dependencies, horizontal resolution is often related to the footprint of the antenna (the area illuminated by the antenna), which is usually estimated as the first Fresnel zone. Different equations are utilized to approximate this zone (Perez-Gracia et al., 2008). Vertical resolution is often considered as ¼ of the wavelength (Dezelic and Apel, 2005; Marcak and Golebiowski, 2008), but in field measurements it is sometimes considered as 1/2 of the wavelength (Schmalz et al., 2002; Al-Qadi and Lahouar, 2005).

Spatial resolution is largely dependent on the beam of the antenna because the footprint of a system at different depths depends on the energy cone transmitted. The beam of the emitted electromagnetic field produces a footprint that varies with depth. The narrower the beam width, the higher the directivity of the antenna and the greater its ability to resolve closely spaced targets in the plane perpendicular to the radiation. The radiation pattern could be considered the directional radiation properties of an antenna in 3D, with the beam being the main lobe of this radiation

pattern. Hence, knowledge of this radiation pattern makes it possible to accurately estimate the antenna's horizontal resolution by estimating the footprint at different depths.

3 Evaluation of the resolution and the beam under lab conditions

3.1 Horizontal resolution

GPR Measurements were carried out in sand, water and air with a commercial 1.6 GHz nominal centre frequency antenna, manufactured by Mala Geosciences. Horizontal resolution was determined using different steel bars configurations embedded in the three different media at different depths. GPR measurements allow to determine the horizontal position of the bars when resolution was available to determine these targets as separated anomalies. Figure 1 shows one of the bars configurations in sand (v=13 cm/ns), together with the radar data obtained in this case. The depth to the bars was 3.5 cm. The anomalies corresponding to the different bars are indicated with arrows in the figure. More cases are extensively presented and discussed in Perez-Gracia et al. (2008).

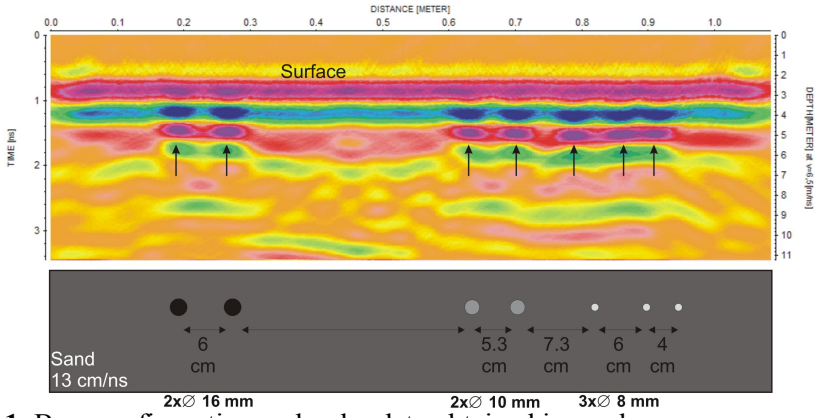

Fig. 1. Bars configuration and radar data obtained in sand.

3.2 Vertical resolution

Vertical resolution was experimentally evaluated for the 1.6 GHz antenna in sand, water and air. In air, the antenna was moved along a polyethylene platform, and a 200 x 200 cm aluminium surface with a slope of about 48.6º was placed under this platform. The propagation velocity was 30 cm/ns. Figure 2 shows a scheme of the experimental device.

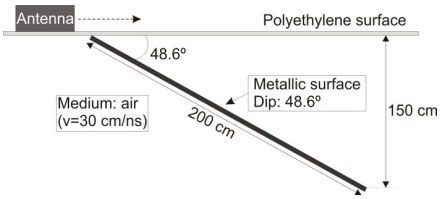

Fig. 2. Experimental device to estimate the vertical resolution in air.

Figure 3a shows that the metallic surface was detected clearly when the distance between the platform and the metallic surface was greater than 20 cm. This distance corresponds to the wavelength in air. For depths smaller than 20 cm, interference effects between the waves made it more difficult to distinguish the exact arrival of the backward wave.

The experimental device in sand and water was similar to those presented in Figure 2. A metallic surface was embedded in the medium. The depth to the metallic surface varies depending on its slope. Figure 3b presents the results obtained in the case of sand with a 11 cm/ns wave velocity. In this case, where the uppermost distance was 2.5 cm, interference effects were observed between the direct and reflected waves on the sand surface (Perez-Gracia et al., 2009).

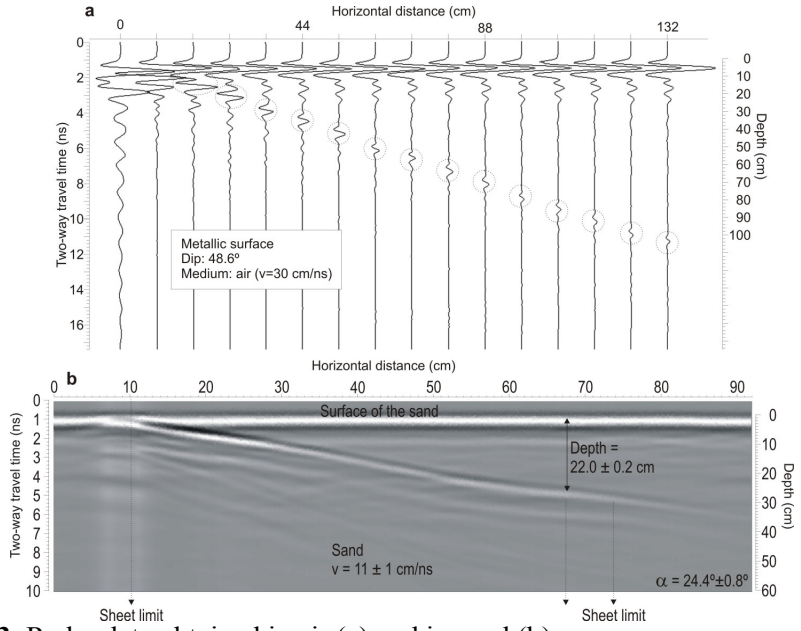

Fig. 3. Radar data obtained in air (a) and in sand (b).

Two different results were considered. The first one was when the reflected wave and the surface-coupled wave were recorded as separated arrivals. In this case, this distance was about 5 cm ($\lambda/2$). The second one was when the radar data

produced an overlap between the reflected and ground-coupled waves, where the arrival of the backward wave was detected. This second result was found for the shallowest part of the metallic sheet, placed at a depth of 2.5 cm (λ/4).

3.3 Beam of the antenna

Furthermore, experimental measurements were carried out in order to determine the beam of the antenna in air. The radiation pattern of an antenna could be considered the directional radiation properties of an antenna in 3D, with the beam being the main lobe of this radiation pattern. Hence, knowledge of this radiation pattern makes it possible to accurately estimate the antenna's horizontal resolution by estimating the footprint at different depths. The beam was experimentally determined measuring the antenna footprint at different depths and considering –37 dB as the limit amplitude and a 40 ns time window. Figure 4 present a 3-D diagram of the antenna beam obtained in air, showing the energy distribution limited by the –37 dB amplitude.

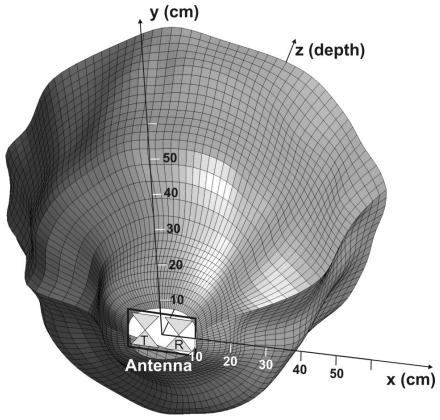

Fig. 4. Boundary of the spatial distribution energy corresponding to –37 dB. The maximum two-way travel time considered was 40 ns. The x axis is the direction of the antenna movement, and the y axis is perpendicular to the antenna displacement.

4 Cases studied

4.1 Detection of underground structures

GPR is widely used to detect structures underneath buildings or historical sites. In these cases, it could be useful to obtain a grid of profiles, covering the whole surface. This kind of data acquisition allows the achievement of time slices and 3-D imaging of the inner medium. Therefore, resolution is also depending on the

distance between profiles, as well as on the scan per meter, the frequency, the energy distribution and the other factors considered in the case of single profiles.

In this example, radar data was acquired in parallel profiles separated 50 cm with a 200 MHz centre frequency RAMAC antenna (Mala Geosciences). Time window was 100 ns and the ground was surveyed with 0.02 scans per centimeter. The wave velocity was calculated to be 8 cm/ns. The subsequent data processing with GPR-Slice software, from Geophysical Archaeometry Laboratory (Goodman, 2004), involved trace marker interpolation, time-zero shift, exponential gain correction, and band-pass filtering. No topographical corrections were needed because the site was quite level. Amplitude time-slice analysis was used in the areas where the grid of profiles was viable. This process is one of the most efficient radar data treatments for interpreting buried features in areas with complex stratigraphy, where it is difficult to associate anomalies with the buried targets. The amplitude time slices are horizontal maps of the recorded amplitudes at different two-way travel times. The time slices were generated at 3 ns intervals using the square of the wave amplitude. They allowed easy visualization of the location, depth, size and shape of the radar anomalies corresponding to buried features. Figure 5 shows four time slices obtained in this survey. In these slices, the most important anomaly could be associated with thick perpendicular walls and with a curved wall. Other thinner anomalies are most likely related to thin walls.

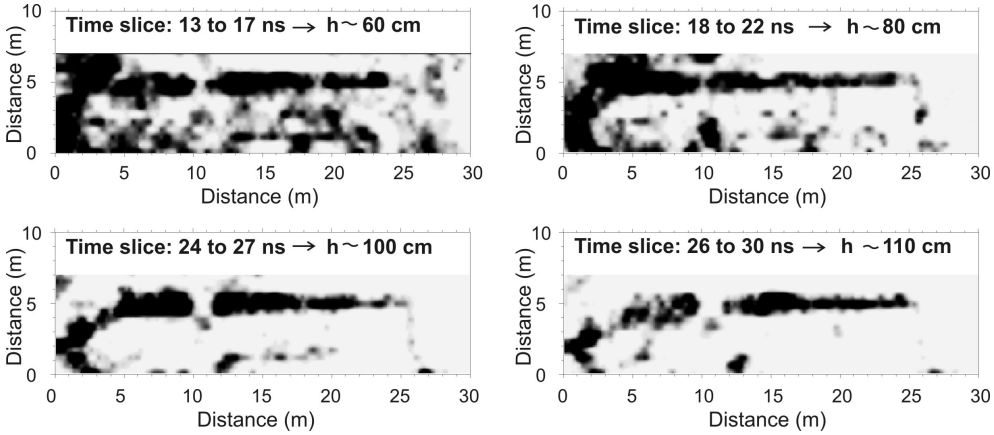

Fig. 5. Time slices obtained with a 200 MHz centre frequency antenna.

4.2 Detection of brick vaults

This example was obtained in the evaluation of an historical building, an old palace today partially rehabilitated. This palace was built as a first square tower. Three adjacent houses were jointed to this palace, presenting different constructive structures (Perez-Gracia et al., 2009). The evaluation was carried out with a 1 GHz nominal centre frequency antenna, being the effective centre frequency of about

750 MHz (λ = 13.3 cm). The wave velocity was highly variable due to the different materials used in the supports, but in the shallowest layers an average velocity seems to be 10 cm/ns. Figure 6 is the radar data and the possible interpretation of the images. In this figure, it is possible to observe an anomaly probably corresponding to a four vaults. In this part of the image, small diffraction hyperbolas become visible most likely between each brick of the vault.

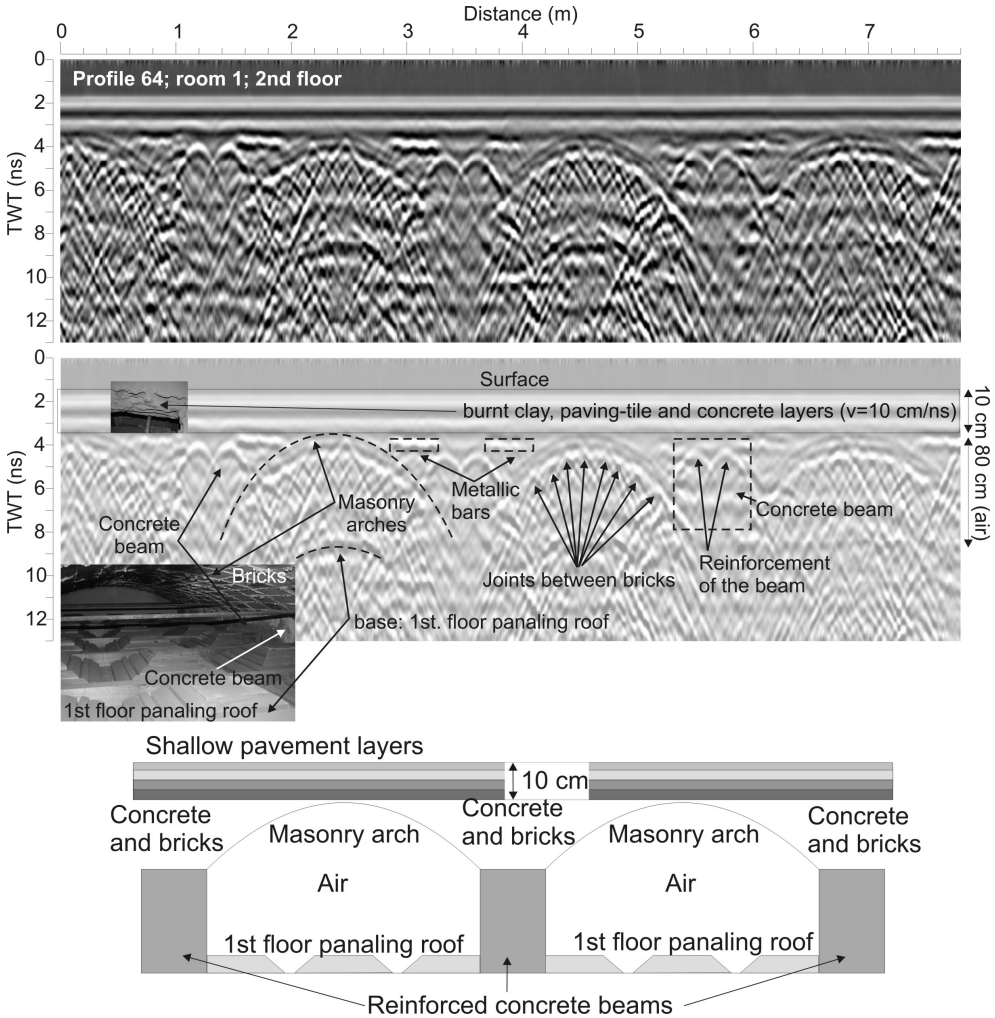

Fig. 6. Radar data and possible interpretation. The vaults are built with bricks. Separation between bricks appear in the radar data as diffraction hyperbolas.

Diffraction hyperbolas between bricks are produced in the corners of these elements. The first branch of the diffraction hyperbolas is caused in the limit of the second brick, and the second branch is caused in the corner of the first brick. This is most likely the cause of the thin shape of these hyperbolas.

4.3 Detection of reinforced slabs in the pavement

Cultural heritage buildings use to be restored and highly modified. In some cases, these restoration are not documented enough. GPR could be useful in the detection of modern reinforced slabs placed in pavements. The example presented in this section (Figure 7) is the detection of a reinforced slab in a pavement. Radar data was obtained with a 1.6 GHz nominal centre frequency antenna, using a grid of parallel profiles separated 3 cm. Radar data acquisition was 0.02 scans per centimetre.

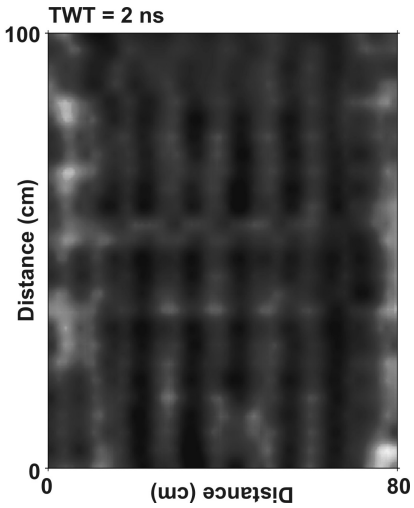

Fig. 7. Slab reinforcement. Higher amplitude reflections in both sides of the image are most likely due to the connection of this reinforcement to the adjacent materials in the pavement.

4.4 Wet reinforced wall

Figure 8a shows an example of the radar data obtained in a reinforced wall with a 1 GHz nominal centre frequency antenna. The antenna was moved parallel to the base of the wall, at a distance to the floor of about 1.5 m. A wave velocity of about 8 cm/ns was obtained from the hyperbolic records. This velocity corresponds to a relative permittivity of 14. This value is considered characteristic of wet concrete, probably presenting high porosity or limestone aggregates. The measured centre frequency is about 620 MHz (Figure 8b), corresponding to a wavelength of 12.9 cm. In the radar data of Figure 5, two different levels of reinforcement are detected. The external one is formed by bars with a free distance of about 20 cm (1.55 λ). The deeper one is like a guide for the shallower reinforcement and bars present a separation of about 1 m (7.75 λ) between them. The covering is of about 3.2 cm (0.25 λ). The distance between the internal and the external reinforcement is about

1.6 cm (0.12 λ). Problematic zones are also observed in both extremes of the radar data. In these cases the reinforcement seems to be moved to an incorrect position. Two possibilities could explain the image in both anomalous zones: changes in the position of the reinforced bars, and changes in the GPR wave velocity due to variations in the concrete properties. Even though, later and punctual invasive measurements seem to indicate that the changes in the properties of concrete wall are insignificant. Then, the possible changes of the electromagnetic properties do not explain these noticeable displacements of the anomalies.

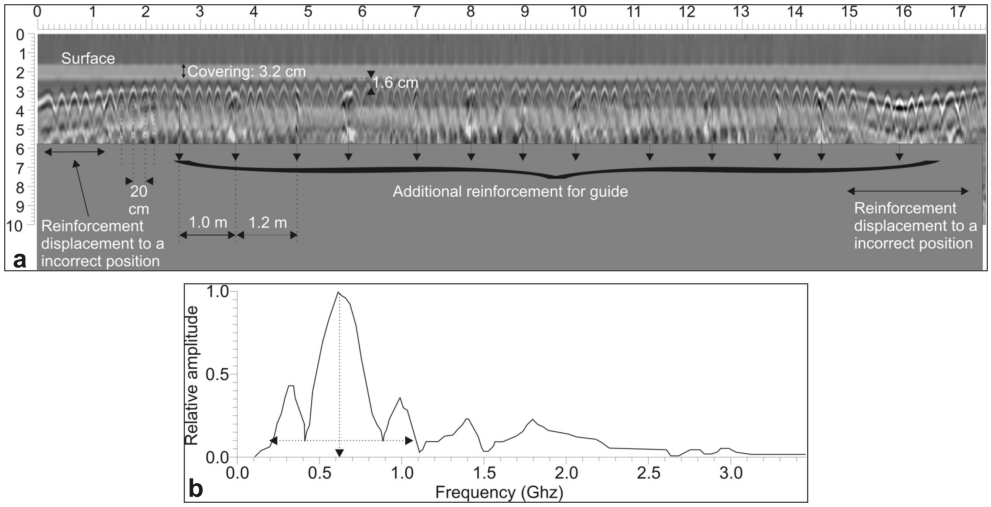

Fig. 8. a) Radar data and possible interpretation. b) Amplitude spectrum showing the average centre frequency of the recorded signal.

4.5 Reinforced pavement

Radar data presented in Figures 9a and 9b were obtained in a reinforced concrete base in a parking zone. GPR was applied in order to obtain a complete map of damages (cracks) and moist areas (see Figure 9c). The average thickness of the slab was 15 cm in the plan. The reinforcement was placed in the bottom of the base, and the distance between bars was 25 cm in plan. No reinforcement exists in the upper part of the slabs. The antenna was 400 MHz nominal centre frequency. The spectrum of the reflected wave presents a centre frequency of about 300 MHz. The measured wave velocity was about 10 cm/ns. Taking into account these considerations, the horizontal distance between bars (25 cm) was 0.75 λ, and the vertical covering distance to the bars (15 cm), 0.45 λ. GPR allows to determine the position of the reinforced bars, to detect cracked zones and the sectors presenting deformation of the slab. In these sections, the vertical distance to the bars was different than 15 cm. Figure 4 shows one of these sectors with a vertical distance of about 11 cm (0.33 λ). GPR also allows to detect changes in the horizontal

separation between bars. It is necessary to consider that resolution in concrete structures depends on the nature of the concrete and, specially, on its conductivity [16]. Higher conductivities produce higher attenuation of the wave and increase the difficult to detect as separated anomalies two adjacent targets.

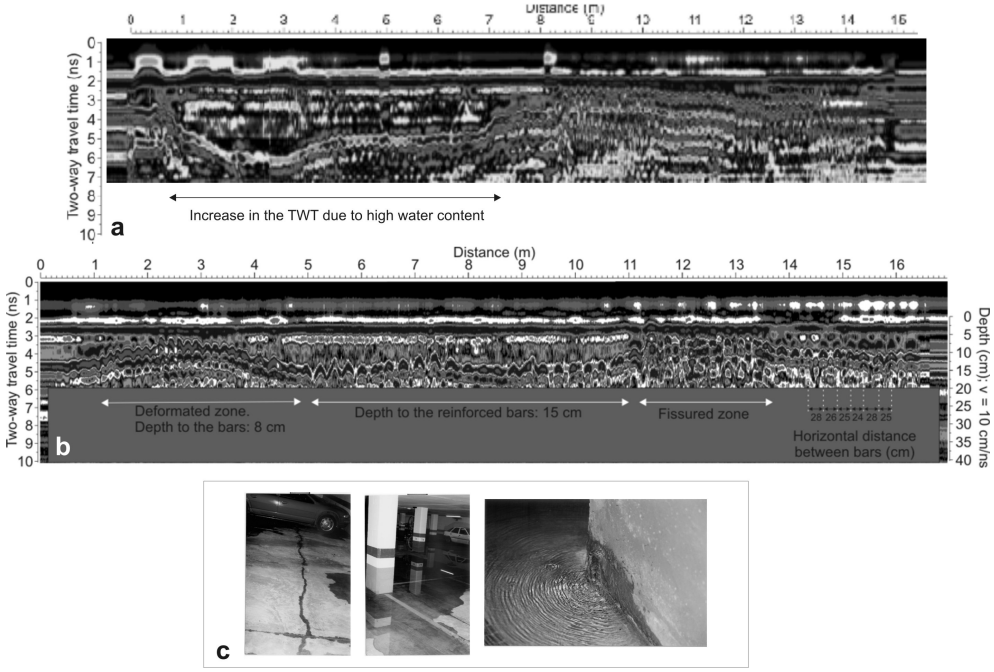

Fig. 9. a) Radar data obtained in a pavement. Changes in the two-way trave time are probably due to changes in the water content. b) Radar data obtained in other profile, showing the distance between bars and different damaged zones. c) Images of the observed damages in the pavement: water and fissures.

5 Conclusions

Experimental measurements in plain media seems to indicate that horizontal resolution could be near to 0.2 λ when the targets are about 0.2 λ deep. Vertical resolution could be considered 0.25 λ. Notwithstanding, resolution depends on the antenna footprint, decreasing with depth.

References

1. Barnes, C. L.: *Linear and nonlinear waves*, Academic Press, 1974
2. Barnes, C. L., Trottier, J.-F., Forgeron, D.: 'Improved concrete bridge deck evaluation

using GPR by accounting for signal depth-amplitude effects', *NDT & E Int.*, 41, 427-433, 2008
3. Hugenschmidt, J.: 'Concrete bridge inspection with a mobile GPR system', *Const. and Building Mat.*, 16, 147-154, 2002
4. Lahouar, S., Al-Qadi, I. L.: 'Automatic detection of multiple pavement layers from GPR data', *NDT & E Int.*, 41, 69-81, 2008
5. Negri, S., Leucci, G.; 'Geophysical investigation of the temple of Apollo (Hierapolis, Turkey) ', *J. of Archaeol. Sci.*, 33, 1505-1513, 2006
6. Perez-Gracia, V., Caselles, O., Clapes, J., Osorio, R., Martines, G., Canas, J.A.: 'Integrated near surface geophysical survey of the Cathedral of Mallorca', *J. of Archaeol. Sci.*, 36, 1289-1299
7. Neal, A., Roberts, C.L.: 'Internal structure of a through blowout, determined from migrated ground-penetrating radar profiles', *Sedimentology*, 48, 791-810, 2001
8. Ghasemi, F.Sh.A., Abrishamian, M.S.: 'A novel method for FDTD numerical GPR imaging of arbitrary shapes based on Fourier transform', *NDT & E Int.*, 40, 140-146, 2007
9. van der Kruk, J.: ' Three-dimensional GPR imaging in the horizontal wavenumber domain for different heights of source and receiver antenna', *Near Surface Geoph.*, 2, 23-29, 2004
10. Daniels, D.J. (editor): *Ground Penetrating Radar. 2nd edition*, IEE Radar, Sonar and Navigation Series 15, Institution of Electrical Engineers, 2004
11. Dezelic, V., Apel, D.B.: ' Evaluation of high frequency ground penetrating radar (GPR) in mapping strata of dolomite and limestone rocks for ripping technique', *Int. J. of Surf. Mining*, Reclamation and Env., 19, 260-275, 2005
12. Marcak, H., Golebiowski, T.: ' Changes of GPR spectra due to the presence of hydrocarbon contamination in the ground', *Acta Geoph.*, 56, 485-504, 2008
13. Schmalz, B., Lennartz, B., Wachsmuth, D.: ' Analyses of soil water content variations and GPR attribute distributions', *J. of Hydrol.*, 267, 217-226, 2002
14. Al-Qadi, I.L., Lahouar, S.: ' Measuring layer thicknesses with GPR – Theory to practice', *Const. and bBuild. Mat.*, 19, 763-772, 2005
15. Perez-Gracia, V., Gonzalez-Drigo, R., Di Capua, D.: ' Horizontal resolution in a non-destructive shallow gpr survey: an experimental evaluation', *NDT & E Int.*, 41, 611-620, 2008
16. Perez-Gracia, V., Di Capua, D., González-Drigo, R., Pujades, L.: ' Laboratory characterization of a gpr antenna for high-resolution testing: radiation pattern and vertical resolution', *NDT & E Int.*, 42, 336-344, 2009
17. Goodman, D.: *GPR-SLICE. Ground Penetrating Radar Imaging Software. User's Manual*, Geophysical Archaeometry Laboratory, California, 2004
18. Perez-Gracia, V., Caselles, O., Clapes, J., Osorio, R., Canas, J.A., Pujades, L.: 'Radar exploration applied to historical buildings: a case study of the Marqués de Llió palace, in Barcelona (Spain) ', *Eng. Fail. Analysis*, 16, 1039-1050, 2009